JOURNAL OF THERMOPHYSICS AND HEAT TRANSFER
Vol. 9, No. 2, April–June 1995

Channel Height and Curvature Effects on Flow Boiling from an Electronic Chip

J. E. Leland*
Wright Laboratory, Wright-Patterson Air Force Base, Ohio 45433
and
L. C. Chow†
University of Kentucky, Lexington, Kentucky 40506

Forced convective boiling from a discrete heat source in a curved rectangular channel has been experimentally investigated. The flow area height and radius of curvature of the channel were varied to ascertain the effects of induced buoyancy and secondary flow. For comparison, results were also obtained for a similar heat source in a straight channel. Three configurations encompassing two radii of curvature, 28.6 and 56.4 mm, and three heights, 3.18, 5.56, and 6.35 mm were studied. An additional channel height of 1.14 mm was investigated for the straight geometry only. Data were obtained for subcoolings of 5, 20, and 35°C and flow velocities of 1–7 m/s. For the straight geometry, critical heat flux (CHF) did not vary much for heights greater than 1.14 mm. The percent increase in curved channel CHF over straight channel CHF was highest for 5°C subcooling. This implies that buoyancy effects are most important when there is significant vapor generation. For a given subcooling and velocity, the radius of curvature had little effect. This implies that secondary flow has little effect under these conditions. A correlation is developed that describes the effects of buoyancy and secondary flow on CHF in the curved channel.

Nomenclature

a = acceleration, U^2/R
C_f = skin friction coefficient
c_p = specific heat at constant pressure
D_h = hydraulic diameter based on wetted perimeter
d_d = bubble departure diameter
f = pressure drop friction factor
g = gravitational acceleration, 9.81 m/s^2
h = channel height
h_{fg} = latent heat of vaporization
It = dimensionless quantity found by Ito,[18] $Re(D_h/2R)^2$
Ja = Jakob number, $c_p\Delta T_{sub}/h_{fg}$
Ja^* = Modified Jakob number, $\rho_f c_p \Delta T_{sub}/\rho_g h_{fg}$
K = Dean number, $Re\sqrt{D_h/2R}$
L = surface heated length
q = heat flux
q_M = critical heat flux
q_M^{**} = dimensionless critical heat flux
R = radius of curvature
R_a = International Organization for Standardization standard (ISO R468) for surface roughness
Re = Reynolds number, UD_h/ν
Ri = Richardson number, $a(\rho_f - \rho_g)L/U^2\rho_f$, where $g = a$ for curved channel flow
T_b = fluid inlet bulk temperature
T_{sat} = saturation temperature based on measured static pressure
T_w = heated surface wall temperature
U = bulk mean velocity based on channel cross section
u = local temporal mean velocity in streamwise direction
u_τ = friction velocity
u^+ = dimensionless velocity, u/u_τ
We = Weber number, $\rho_f U^2 L/\sigma$
w = channel width
y = distance outward normal from heater
y^+ = dimensionless wall coordinate, yu_τ/ν
ΔT_{sub} = subcooling, $T_{sat} - T_b$
μ = dynamic viscosity
ν = kinematic viscosity
ρ = density
σ = surface tension

Subscripts
b = bubble
cur = curved section
f = liquid
g = vapor
str = straight section

Presented as Paper 92-0250 at the AIAA 30th Aerospace Sciences Meeting and Exhibit, Reno, NV, Jan. 6–9, 1992; received Oct. 30, 1992; revision received Sept. 12, 1994; accepted for publication Sept. 13, 1994.

*Research Engineer, Aerospace Power Division. Member AIAA.
†Professor, Department of Mechanical Engineering. Associate Fellow AIAA.

Introduction

A VAST amount of experimental work has been performed in an effort to develop means of cooling the high-speed, large-scale integrated circuits envisioned to be in service by the mid-1990s. Heat fluxes of 100 W/cm^2 and maximum chip operating temperatures of 85°C are often predicted. An excellent review of this work was performed by Incropera.[1] Some military power conditioning applications require heat fluxes in excess of 500 W/cm^2. Most studies have concentrated on boiling heat transfer using an inert fluorocarbon, FC-72 (3M Industrial Chemical Products Division). FC-72 is used because of its dielectric properties and because its boiling characteristics correspond to desired chip operating temperatures. The heat transport properties of FC-72 are poor however, compared to water and the soon to be banned R-113, a comparable chlorofluorocarbon. Thus, boiling enhancement schemes such as curved channel are being pursued.

The high critical heat flux (17 kW/cm^2 using water) capabilities of flow boiling over a concave surface have been known since the work of Gambill and Greene.[2] Gambill and Greene[2] attributed the effectiveness of their strategy to the increased

Table 1 Flow channel parameters and geometry factor

Channel	1	2	3	2 c/shim
R	56.4 mm	28.6 mm	28.6 mm	∞
w	27.0 mm	27.0 mm	27.0 mm	27.0 mm
h	5.56 mm	3.18 mm	6.35 mm	1.14 mm
L	9.52 mm	9.52 mm	9.52 mm	9.52 mm
D_h	8.91 mm	5.68 mm	10.3 mm	2.19 mm
$(L/D_h)^{1/25}$	1.0029	1.0227	0.9967	1.0659

inward radial transport of bubbles caused by increased buoyant forces due to the centrifugal acceleration of the fluid. They achieved more than a threefold increase over a comparable straight geometry for an induced acceleration of 8390 g. Recently, Leslie et al.[3] reported heat fluxes of 25 kW/cm^2 for water in another concave geometry.

Miropol'skiy and Pikus[4] obtained CHF data for water flowing in a heated 360-deg tube coil. They found that with increasing heat input, CHF first occurred on the inner radius and then (at a much higher heat input), on the outer radius of the bend. For subcooled and low quality flow, CHF (averaged over the tube circumference), was less than that for a straight tube of equal diameter. At higher qualities, the reverse was true. Higher heat transfer rates on the outer portion of the tube circumference for high-quality flow was attributed to secondary flows. A significant factor of heat transfer in curved ducts is secondary flow. As a tube flow with a typical laminar or turbulent velocity profile enters a bend, the higher velocity fluid in the core attains a larger radial momentum. The core fluid moves to the radially outward wall and then migrates along the pipe wall to the radially inward area of the wall. Secondary flows are typically less vigorous for turbulent flow because of the flatter velocity profile. The flow was turbulent ($Re = 9 \times 10^3$ to 2×10^5), for the entire range of conditions of this investigation.

Hughes[5] has obtained results for a 90-deg bend of square cross section with a thin heater on each of the walls normal to the radial direction. Results were obtained for only one heater operating at a time. Hughes does not give the heater dimensions, but they are estimated to be 3 mm wide by 100 and 120 mm in length for the inner and outer surfaces, respectively. Hughes' results imply that CHF becomes independent of a/g for accelerations ratios greater than 20. Furthermore, the ratio of outer wall CHF to straight channel CHF decreases from roughly 1.6 to 1.3 for subcoolings of 10 and 43°C, respectively. It may be concluded from the foregoing studies that curved channel boiling is most effective when there is significant vapor generation.

Gu et al.[6] obtained results for a simulated electronic chip in a curved rectangular channel. CHF was found to increase 8 and 44% over results for a straight channel at velocities of 1 and 4 m/s, respectively. This geometry is similar to that of the present study and is quite different from those previously studied.[1-5] In an effort to determine the effects of centrifugal force and secondary flow, the present results have been obtained for three test sections with dimensions shown in Table 1.

Experimental Apparatus

The experimental apparatus has three primary components: 1) the flow loop, 2) flow channel, and 3) heater test section. Details of the flow loop have been previously described by Leland and Chow.[7] Figure 1 shows the general design of the three test sections or flow channels. The entrance length is greater than 20 hydraulic diameters in all cases to insure fully developed flow. The curved section heater was placed 135 deg from the bend entrance where the secondary flow is believed to be fully developed. Literature on turbulent flow in curved channels of square cross section is scarce. The few studies[8-10] that do exist indicate that the nature of secondary flow, (two counter-rotating vortices in the plane perpendicular to the streamwise direction), is established well before 90 deg, and is well developed at 135 deg.

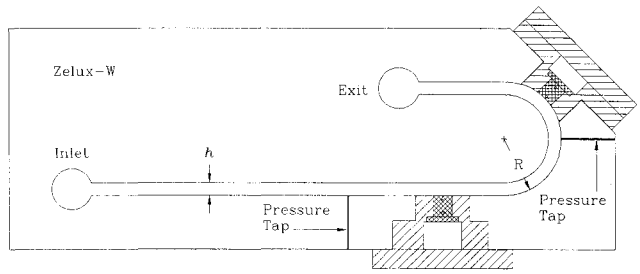

Fig. 1 Flow channel design.

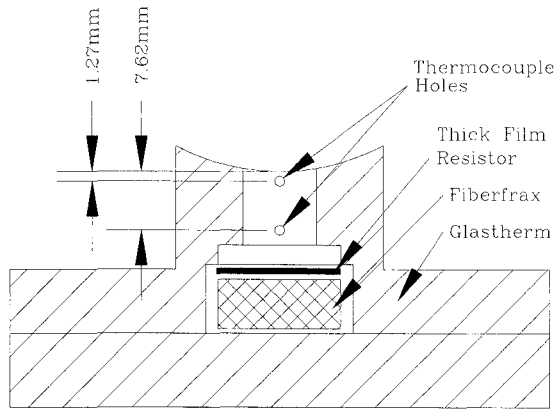

Fig. 2 Test heater and enclosure.

The channel was rotated so that the heater surfaces could be maintained in a vertical orientation with the flow direction being upward. Orientation to gravity was found to have little effect on the results for the straight section heater and velocities greater than 2 m/s. The effect of orientation on the curved section heater results is presumed to be similar. The channels were made of Zelux-W optical grade plastic for the purpose of flow visualization.

Static pressure measurements are made at the channel wall at a distance of 35 mm upstream of each straight section heater leading edge. This distance was 33 and 23 mm for the 56.4 and 28.6 mm radius curved sections, respectively. The saturation temperature at the heater surface is based on the static pressure measurement, thus a small error in saturation temperature is incurred because of the pressure drop from the point of measurement to the heater surface. The bulk temperature is measured at a point 40–50 mm upstream of the straight section heater. Temperature drop from the point of measurement to the test heater is negligible as confirmed by measurements taken at the test section exit with both heaters off. High- and low-range turbine flow meters were used for the determination of the bulk velocity.

An oxygen-free copper block was used to simulate an electronic device and is shown in Fig. 2. The copper block was enclosed in low thermal conductivity (0.3 W/m-K) Glastherm HT (General Electric Corp.) and heated from the back side. Two actual heater designs were employed. For the straight section and the curved section of channel no. 1, the copper block was heated by a nichrome wire sandwiched between two plates of boron nitrate (65 W/m-K). For the curved section heater of channel nos. 2 and 3, a thick film resistor (Emtron Corp.) was used to heat the copper block. The thick film resistor could be soldered directly to the copper block, thus reducing the contact resistance and operating temperature of the heater. Because of the temperature limitations of the Glastherm HT, CHF values could not be obtained with channel no. 1 for higher velocities. Note that the same heater enclosure was used for the straight segment of all flow chan-

nels and the same test heater and enclosure was used for the curved segments of channel nos. 2 and 3. The thermocouple locations for the straight section heater are the same as those for the curve section heater (Fig. 2).

Great care was taken to insure that the copper surface was flush with the wall of the flow channel. Gu et al.[6] reported a significant reduction of CHF for surfaces that were slightly (≈0.1 mm) below or above the flow channel wall. The effect of surface height was studied in detail by Leland and Chow.[7] Care was also taken to ensure that the sides of the copper block sealed well against the Glastherm enclosure. High-temperature silicone sealant was used for this purpose. Two 0.51-mm-diam type K thermocouples were imbedded in the block through 0.57-mm-diam holes and a one-dimensional approximation of heat conduction was made to calculate heat flux. Heat loss, which occurred predominantly through the back of the enclosure, was about 10% near CHF for a flow velocity of 1 m/s and decreased slightly as heat flux increased. The heater enclosure with the thick film resistor showed a loss of about 2% less owing to the lower operating temperature.

Experimental Procedure

Before installation into the enclosure, the exposed face of the copper block was sanded in alternate directions with 1000 grit Wetordry (3M Corp.). Measurements with a surface profilometer confirmed that surface roughness was uniform over the entire face. A Taylor-Hobson profilometer was used to measure the surface roughness of the various test heaters. Eight measurements at various surface locations were taken to obtain an average roughness for each heater surface. R_a, an ISO standard parameter for surface roughness, was obtained as the average of five 50-μm sampling lengths. Although larger sampling lengths did not yield vastly different values of R_a, this small sampling length was used because the expected nucleation cavity size was expected to be much smaller than 50 μm. The previously described sanding technique provided very uniform surfaces because R_a was found to range from only 3 to 6 nm for the entire set of surfaces with a single surface R_a variance of ± 1 nm. Further details of the experimental procedure have been previously described by Leland and Chow.[7]

Uncertainty Analysis

For all tests, CHF was calculated from the one-dimensional heat conduction equation. Because the Seebeck coefficient is nearly constant over the temperature range (20–150°C) of the experiments, the temperature difference of two type K thermocouples was measured directly, to obtain a higher accuracy. Furthermore, the measured gradient was always less than 20°C, making the constant Seebeck coefficient assumption a good one. For all test heaters, the thermocouple pairs were compared to a precision thermistor (0.1°C accuracy) over the temperature range of the experiments. The thermocouples of each pair agreed to within 0.3°C over the entire temperature range. All the thermocouples agreed with the precision thermistor to within 0.5°C. Thus, the thermocouple accuracies are considered to be well within 1°C for these experiments. A Helios I (John Fluke Mfg.) data acquisition system was used for these measurements. This device has a resolution of 0.02°C and a rated accuracy of 0.45°C for K type thermocouples.

The uncertainty of the pressure measurement was 5 Pa. The error induced by the pressure taps being upstream of the heater was estimated to range from 70 Pa at $U = 1$ m/s to 2.36 kPa at $U = 5$ m/s. This range was nearly the same for both the straight and curved sections of each channels because the pressure drop distance in the curved sections was shorter to compensate for the larger friction factor. The resulting error in saturation temperature was less than 0.5°C for both the straight and curved sections. The uncertainty of the bulk mean velocity calculation was dominated by the uncertainty of the turbine flow meter, which was 0.5% of the reading.

The standard Kline and McClintock[11] approach to the calculation of random uncertainty was taken. Because temperature difference is the only variable during testing, the uncertainty in CHF decreases monotonically with temperature difference or heat flux. The uncertainty in CHF was calculated for best and worst case temperature difference uncertainties of 0.5 and 1°C. For a temperature difference uncertainty of 0.5°C, the uncertainties in CHF are 13.4, 7.8, and 6.9% for heat fluxes of 34, 85, and 132 W/cm^2, respectively. For a 1°C uncertainty, the uncertainties in CHF are 24.5, 11.3, and 8.7% for the same heat fluxes.

Previous results[12] give a maximum upstream to downstream temperature difference of only 2.2°C for a flush-mounted copper heater under similar heat flux, subcooling, and flow conditions. Because of this, additional thermocouples to obtain the surface temperature distribution were considered an unnecessary complexity, and were not used. Because of the high thermal diffusivity of copper and the distances of the thermocouples from the boiling surface, the measured temperatures, and thus the calculated heat flux and wall temperature, fluctuated very little under all conditions. The maximum unsteadiness (less than 0.1°C) occurred near CHF and translates into a heat flux variance of less than 1 W/cm^2.

Nevertheless, Kenning[13] has shown that large errors may occur in the surface temperature measurement of boiling surfaces. These errors are caused by the large variation in heat flux below a single bubble at a nucleation site. He developed a conduction model of the spatial temperature variation that required the fitting of two constants, a and b, to his data. Results obtained by applying Kenning's[13] model to the present experiment show that for all practical values of a and b, thermal gradients disappeared at a distance of about one bubble diameter (i.e., <0.1 mm) below the surface. High bubble density, small maximum bubble diameters, and the high thermal conductivity of copper are the reasons for a negligible temperature variation. Thus, the small unsteadiness of the thermocouple closest to the boiling surface is expected.

A precision shunt with a resistance uncertainty of 0.05% was used to calculate CHF based on electrical power input. For the worst case, the random uncertainty of this value was less than 0.3%. Because the CHF based on thermocouple measurement was always within 7–10% of that based on electrical input, it is believed that the actual uncertainty of the thermocouple measurements is less than calculated. The use of the same heater and enclosure for all straight sections and two of the three curved sections also increases the accuracy of the comparative results. The repeatability of CHF values was generally within 5% for heat fluxes greater than 50 W/cm^2. Finally, the bias error was not estimated, however, the percentage of heat loss measured compares with that previously reported for a similar design.[12]

Results

Results were obtained for velocities of 1–7 m/s, and three subcoolings, 5, 20, and 35°C. Three test sections (see Table 1) offered channel heights of 3.18, 5.56, and 6.35 mm. Data for a height of 1.14 mm were obtained by insertion of a shim into the straight section flow path of channel no. 2. The flow was well within the turbulent regime for all cases.

Effect of Channel Height

A series of data was obtained to determine the effect of channel height on CHF for the straight section heated surface. Channel height was initially varied to change the magnitude of secondary flow in the curved channel. In order to separate the effects of secondary flow and channel height alone, the latter was studied for the straight section. Figure 3 illustrates the effects of velocity, subcooling, and channel height. It is readily seen that there is little difference for heights of 3.18 to 6.35 mm. However, as h is reduced to 1.14 mm, a significant change of q_M is observed. For this height, the CHF was in-

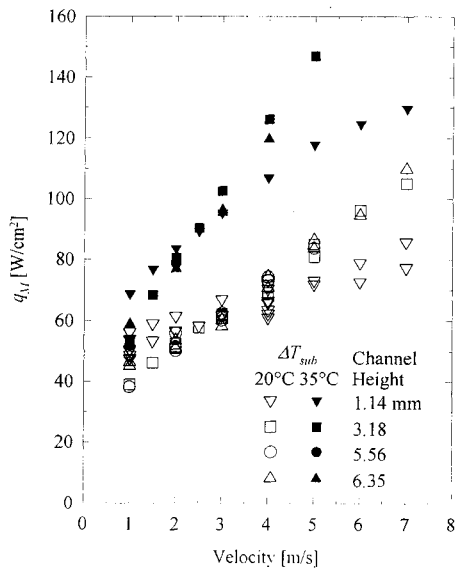

Fig. 3 Effect of velocity, subcooling, and height.

creased for velocities less than 3 m/s and reduced for velocities greater than 3 m/s as compared to results for heights of 3.18–6.35 mm.

Mudawar and Maddox[12] obtained similar data for velocity and subcooling ranges of 0.22–4.1 m/s and 0–44°C, respectively. They developed the following predictive correlation based on a physical model of CHF:

$$q_M^{**} = 1.052\psi^{8/23} We^{-8/23} \tag{1}$$

where

$$q_M^{**} = \frac{q_M/U\rho_g h_{fg}}{(\rho_f/\rho_g)^{15/23}(L/D_h)^{1/23}[1 + Ja]^{7/23}[1 + C_{sub}Ja^*]^{16/23}} \tag{2}$$

and values for the group

$$1.052\psi^{8/23} = 0.161 \tag{3}$$

and the constant

$$C_{sub} = 0.021 \tag{4}$$

were found to fit the data for the range $We^{-1} > 10^{-4}$. At near atmospheric pressure, this corresponds to velocities of about 2 m/s or less. The present data are plotted against Eq. (1) in Figs. 4 and 5 for subcoolings of 20 and 35°C, respectively. Noting that for $h \geq 3.18$ and $We^{-1} > 10^{-4}$, the data fall predominantly below the line for 20°C subcooling and above the line for 35°C subcooling, Eq. (1) does not collapse the data with respect to subcooling as well as for the data of Mudawar and Maddox.[12] However, the dependence on velocity is in good agreement with that of Mudawar and Maddox.[12]

Equation (2) indicates a geometry dependence of $(L/D_h)^{1/23}$ on q_M. Thus, q_M increases weakly as D_h decreases. Note that this trend is counter to what is generally found for single-phase convection. The precise values of $(L/D_h)^{1/23}$ are given in Table 1. Table 1 indicates that q_M may be expected to increase 7% as the term, $(L/D_h)^{1/23}$, varies from 0.9967 (largest h) to 1.0659 (smallest h). Figure 3 clearly indicates that an even greater enhancement is realized over the range of validity of Eq. (1). Much more interesting is the nature of CHF as nondimensionalized in Figs. 4 and 5. While the data for $h = 3.16$, 5.56, and 6.35 mm compare to previously reported results (Leland and Chow[7] and Mudawar and Maddox[12]),

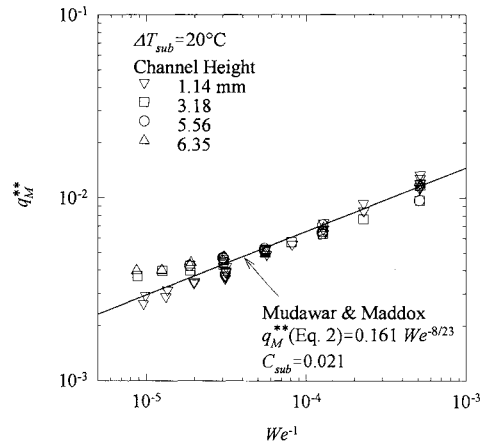

Fig. 4 Comparison of data with Eqs. (1–4).

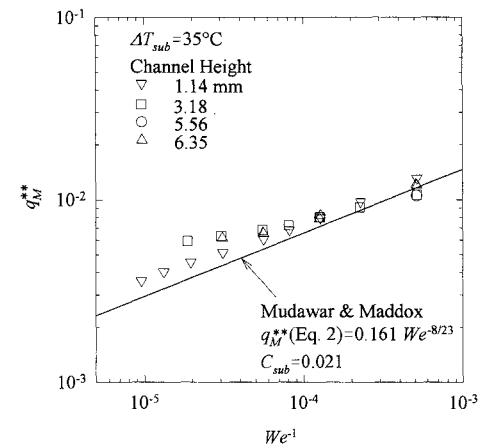

Fig. 5 Comparison of data with Eqs. (1–4).

the data for $h = 1.14$ mm compares well to Eq. (1) throughout the entire range of We^{-1}.

To understand why this is true, one must consider the CHF mechanism upon which Eqs. (1) and (2) are based. CHF occurs when the liquid sublayer below the bubble vapor blanket dries out. Mudawar and Maddox[12] found that for velocities of 1 to 2 m/s, liquid was fed tangential to the surface from the leading edge of the heater. Since the vapor blanket grows in thickness with the direction of flow, the liquid supply to the most downstream portion of the heater is the most impeded. Thus, dryout initially occurs at the most downstream portion of the heater. This is the mechanism upon which Eqs. (1) and (2) are based.

At higher velocities, the vapor blanket is much thinner and more uniform in thickness over the length of the heater. Mudawar and Maddox[12] described the existence of vapor blankets prior to CHF that were much smaller in size than the heated surface area. The liquid sublayer beneath these blankets was fed by liquid from above and between the blankets instead of from the leading edge of the heater. Because the sublayer is more uniformly fed over the length of the heater, the transition to CHF is delayed and higher heat fluxes are attained (see Figs. 4 and 5).

For the case of $h = 1.14$ mm, the bubble layer thickness is of the same order as h. Thus, the liquid flow from above the vapor blanket is impeded and the first mechanism remains at higher velocities. Note that the two sets of data cross at $We^{-1} \approx 10^{-4}$, the same point at which the transition from the low to high velocity mechanism occurs. This does not explain the increase of q_M^{**} for $We^{-1} > 10^{-4}$. The vapor blanket is thickest at low velocities and approaches h near CHF for $U = 1$ m/s and $h = 1.14$ mm. A significant fraction of the flow area is thus blocked and the flow may be accel-

erated by as much as 50%. Inspection of Fig. 4 indicates that this may be true. The uncharacteristic scatter in the data for $h = 1.14$ mm cannot be explained except to say that boiling throughout the nucleate boiling regime and near CHF was less stable, causing CHF to be less repeatable.

McGillis et al.[14] also studied the effect of channel height on boiling. They compared the results of three channel heights, 6.4, 3.2, and 1.9 mm, and found no change of q_M. Their results are for the most downstream of 10 heat sources and flow velocities less than 0.25 m/s. As reported,[14] a CHF mechanism closer to that of pool boiling exists at these low velocities. The effect of h may be obscured by the vapor generated by the nine downstream heaters. A generous amount of vapor may cause a smaller boost in velocity. Alternatively, the effect of h may diminish with the change in CHF mechanism.

Effect of Radius of Curvature

Figures 6 and 7 show how CHF varies with subcooling, flow velocity, and channel geometry. For the purpose of clarity, the straight section data is the average of those values for $h = 3.18$, 5.56, and 6.35 mm, and the curve section data is the average value for each velocity and subcooling. It should be noted that heat flux is based on the exposed heated surface rather than the cross-sectional area for the curved section heater. This correction is small however, because the ratio of the surface area to the cross-sectional area is only 1.004. In all cases but one, channel curvature has a positive effect on CHF. Channel curvature has a detrimental effect for $R = 28.6$ mm, $h = 3.18$ mm, and $\Delta T_{sub} = 35$°C. The results of Gu et al.[6] show that compared to the data of Fig. 6, much greater increases were obtained for velocities of 3 and 4 m/s. Their results may be in error, however, due to the investigators' assumption that the test section pressure was constant and equal to the ambient pressure plus the static head of the fluid. Although this assumption is acceptable for low flow rates, the absolute system pressure can increase by as much as 0.5 atm for a flow velocity of 5 m/s. This would lead to greater than 10°C under-reporting of the subcooling. Nonetheless, this error would occur for both the straight and curved section heaters, thus lending some credibility to their results. Figures 6 and 7 show that any increase of the CHF due to channel curvature diminishes with increasing subcooling. The top portion of Fig. 7 also shows how the data compare to Eqs. (1–4).

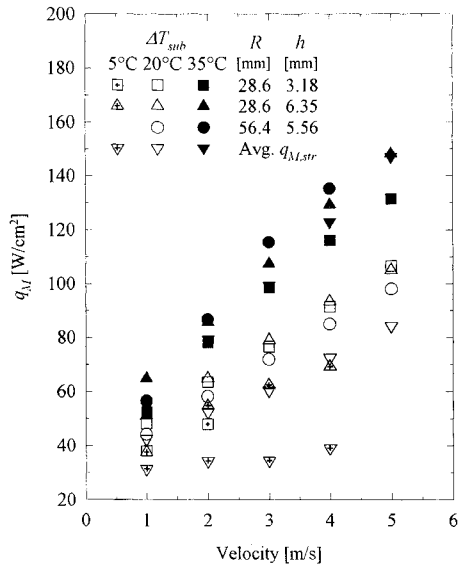

Fig. 6 Comparison of CHF for straight and curved sections.

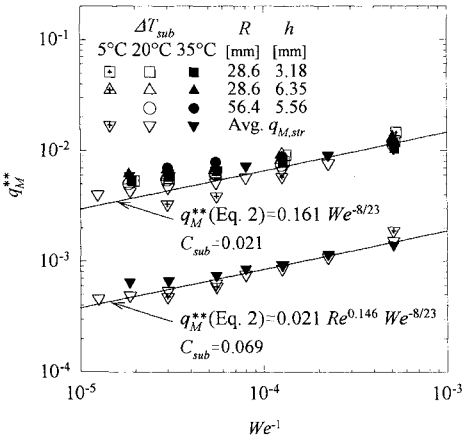

Fig. 7 Comparison of q_M^{**}, Eq. (2), for straight and curved sections.

The effects of channel curvature on nucleate boiling manifest in three ways: 1) increased buoyant forces, 2) the establishment of secondary flow, and 3) increased wall shear stresses on the outer wall that yield a higher fluid velocity gradient near the wall. Increased buoyant forces can cause the vapor to escape from the heated surface more rapidly, thus improving the ability of liquid to wet the surface. This is the mechanism that Gambill and Greene[2] attributed their extremely high heat fluxes to. Because CHF occurs as a result of liquid flow being impeded by the bubble layer, it was concluded that increased buoyant forces would cause the bubbles to leave the surface much more quickly, thus increasing the CHF. For the present experiments, buoyancy is a function of U^2/R. Large buoyant forces may also have a detrimental effect on CHF. As a result of pool boiling experiments under high acceleration, Ulucakli and Merte[15] have postulated that increased buoyant forces cause attached bubbles to elongate and thus increase the microlayer thickness below the bubble. This theory was used to explain the increase of wall superheat at higher levels of heat flux for increasing gravity. A reduction of wall superheat with increasing gravity was found at low levels of heat flux. Although their investigation did not include the effects on CHF, an increased wall superheat could cause premature dryout of the sublayer.

Another manifestation of curved channel flow is secondary flow. When a fluid enters a curved duct, the sudden change in direction causes high velocity, large momentum fluid in the core to be driven radially outward toward the heated surface. This condition aids in driving liquid through the bubble layer to the wall, but may also tend to drive bubbles back towards the wall. Although it is a weak indicator of turbulent secondary flows, the Dean number K is still sometimes used in turbulent single-phase heat transfer correlations. For a given velocity, K is 2.6 and 1.75 times greater for $R = 28.6$ mm and $h = 6.35$ mm than for $R = 28.6$ mm and $h = 3.18$ mm, and $R = 56.4$ mm and $h = 5.68$ mm, respectively. Finally, channel curvature causes higher velocity gradients at the outer wall. Thus, higher velocity fluid feeds the sublayer for the curved channel as compared to the straight channel for the same bulk velocity. Higher velocity fluid near the wall provides improved wetting of the surface, and therefore, increases the CHF. This third consequence of curved channel flow can be accounted for by a modified version of the Mudawar and Maddox[12] model. Equations (1) and (2) may be rederived considering the velocity profile for the curved channel.

Velocity data for curved channels of rectangular cross section are very scarce and a "law of the wall" does not exist for the curved channel. Marris[16] found that Reynolds similarity of the streamwise velocity profiles does exist for a square channel with a mean radius to width ratio R/h of 5.9 and $Re = 4.2 \times 10^4$ to 1.39×10^5. But experiments for a smaller mean radius to width ratio of 2.1 showed that Reynolds similarity of the velocity profiles was lost. The mean radius to

Table 2 Change of velocity profile, buoyancy, and secondary flow with velocity

	Parameter								
	$It^{1/115}$, channel			a, m/s^2, channel			$K \times 10^{-3}$, channel		
	1	2	3	1	2	3	1	2	3
U = 1 m/s	1.048	1.048	1.064	18	35	35	9.9	6.6	16.4
U = 2 m/s	1.055	1.054	1.070	71	140	140	20.1	13.3	33.1
U = 3 m/s	1.059	1.058	1.074	160	315	315	30.6	20.6	50.4
U = 4 m/s	1.062	1.061	1.077	284	559	559	41.8	27.8	68.8
U = 5 m/s	1.064	1.063	1.080	443	874	874	53.7	34.8	88.5

width ratios of the current experiments are 10.1, 9.0, and 4.5 for channels 1, 2, and 3, respectively, and a similar range of Re. Ellis and Joubert[17] have also shown experimentally that velocity profiles for the curved channel do follow the law of the wall up to $y^+ = 200$ for values of Ru_τ/ν greater than 4×10^4. Note that as $R \rightarrow \infty$, the straight flow velocity profile is obtained. For the current experiments, Ru_τ/ν ranges from 5×10^3 to 2×10^4, which will cause the velocity profile to depart from the law of the wall at a y^+ less than 200. Despite this, $y^+ = 200$ is equivalent to a wall coordinate of about 0.75 to 0.35 mm for velocities of 1 to 2.5 m/s, [the valid range of Eqs. (1) and (2), for the conditions of the present experiments]. Because the bubble layer thickness ranges from about 1 to 0.5 mm (low to high velocity), it is assumed that the law of the wall velocity profile is applicable for the following analysis. This assumption will yield conservative estimates of the velocity profile. Proceeding similar to Mudawar and Maddox,[12] a derivation of a curved channel counterpart to Eqs. (1) and (2) is briefly described as follows. First a sublayer dryout criteria is written

$$q_M L = \rho_f (c_p \Delta T_{\text{sub}} + h_{fg}) \int_0^{\delta_M} u \, dy \tag{5}$$

where δ_M is the liquid sublayer thickness that is completely transformed to vapor. The velocity profile is obtained from the power-law form of the law of the wall or

$$u^+ = 8.56 y^{+1/7} \tag{6}$$

where

$$u^+ = u/u_\tau = \sqrt{C_{f_{\text{cur}}}/2} \tag{7}$$

At this point, the effect of wall curvature is introduced through Ito's[18] relation for the curved pipe friction factor, or

$$f_{\text{cur}}/f_{\text{str}} = [Re(D_h/2R)^2]^{1/20} \tag{8}$$

Using the Blasius solution, $f_{\text{str}} = 0.316 Re^{-1/4}$, and assuming $C_f = f/4$, Eq. (5) may be integrated to obtain

$$\frac{q_M}{U\rho_g h_{fg}} = 1.183 \left(\frac{\rho_f}{\rho_g}\right) \left(1 + \frac{c_p \Delta T_{\text{sub}}}{h_{fg}}\right) \left(\frac{L}{D_h}\right)^{1/7} \times \left(\frac{\delta_M}{L}\right)^{8/7} \left[Re \left(\frac{D_h}{2R}\right)^2\right]^{1/35} \tag{9}$$

where the last bracketed term is the only change from the straight channel derivation. Note the similarity of this term to the Dean number. The remaining unknown, δ_M, may be obtained from an equation based on a Helmholtz instability criteria for planar flow of liquid and vapor

$$\frac{\delta_M}{L} = \psi \left(\frac{\rho_f}{\rho_g}\right) \frac{(\sigma/\rho_f U^2 L)}{(q_M/U\rho_g h_{fg})^2} \left(1 + C_{\text{sub}} \frac{\rho_f c_p \Delta T_{\text{sub}}}{\rho_g h_{fg}}\right)^2 \tag{10}$$

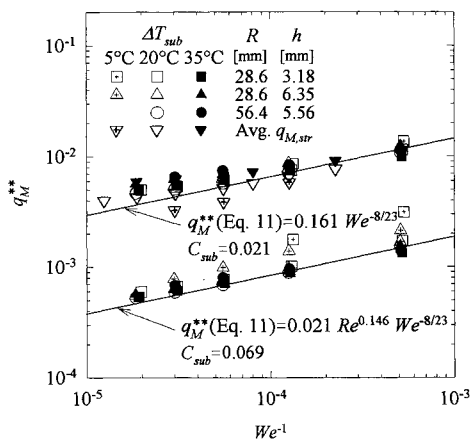

Fig. 8 Comparison of q_M^{**}, Eq. (11), for straight and curved sections.

where ψ is a constant. The derivation of this equation is described at length in Refs. 12 and 19. Combining Eqs. (9) and (10) gives Eq. (1) and

$$q_M^{**} = \frac{q_M/U\rho_g h_{fg}}{(\rho_f/\rho_g)^{15/23}(L/D_h)^{1/23}[1 + Ja]^{7/23}[1 + C_{\text{sub}} Ja^*]^{16/23} It^{1/115}} \tag{11}$$

where $It = Re(D_h/2R)^2$. Note the addition of the term It in the denominator of Eq. (11) is the only difference from Eq. (2). Although any quantity to the power 1/115 would appear insignificant, Re is very large relative to the other factors in the denominator. To see the effect of the curvature term on q_M directly, $It^{1/115}$ is evaluated and presented in Table 2.

It can be seen that not much difference can be expected over the range of geometries and velocities explored, even though the aforementioned Dean number and buoyancy forces change dramatically (cf. Table 2). The values of $It^{1/115}$ indicate an increase of q_M of only 5–8% over the range of velocities, subcoolings, and geometries explored. Figure 8, (top plot), shows the data of Fig. 7 replotted using Eqs. (1) and (11) for the curved channel data. The data are only slightly closer to the correlation, thus illustrating the limited ability of Eq. (11) to account for channel curvature.

The above three effects of channel curvature on CHF are coupled and may work with or against each other in enhancing the CHF. Further complicating the understanding of the effects of channel curvature is the fact that a transition in the liquid supply mechanism occurs within the range of velocities studied. Nonetheless, in order to increase buoyant forces, secondary flow, or the velocity gradient near the outer wall, either D_h must be increased or R must be decreased. Neither alternative is attractive from a manufacturing point of view. Increasing D_h will yield a large flow channel, thus increasing pumping power, and reducing R may necessitate making a chip with a curved surface.

Figure 9 shows more clearly the effects of channel curvature and subcooling on the CHF. As subcooling decreases, the

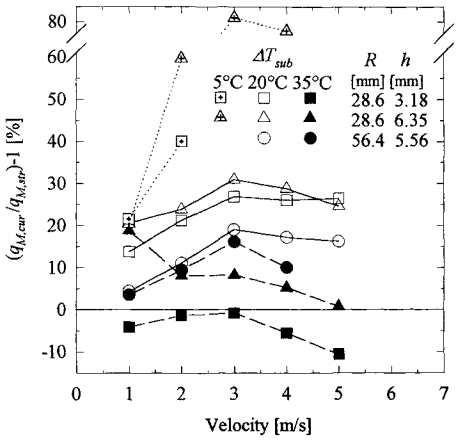

Fig. 9 Relative difference of $q_{M,cur}$ and $q_{M,str}$.

increase in $q_{M,cur}$ over $q_{M,str}$ increases. For $\Delta T_{sub} = 20$°C, the percent increase of $q_{M,cur}$ over $q_{M,str}$ for the two 28.6-mm channels is roughly twice that of the 56.4 mm radius. If secondary flow is considered to enhance CHF, the results for channel no. 1 ($R = 56.4$ mm) should be greater than those for channel no. 2 and less than those for channel no. 3. The effects on CHF of secondary flow and wall shear stresses should not change appreciably with the level of subcooling. Buoyant forces do change with subcooling, however. As subcooling increases, bubble departure sizes decrease, thus causing buoyant forces to decrease. All of this implies that buoyant forces are the dominant contributor to increased CHF at lower subcoolings.

It may also be seen that, in general, for a given subcooling and geometry, the effect of buoyancy decreases with increasing velocity for $U > 3$ m/s. This may be due to thickening of the bubble microlayer, the effects of which were discussed above. Alternatively, increasing secondary flow may be forcing bubbles back towards the surface, thus impeding the liquid supply mechanism. Finally, the transition from increasing to decreasing percent enhancement occurs near the velocity for which there is a transition in the liquid supply mechanism. It is therefore difficult to draw any conclusions for this trend.

Figure 9 also shows that wall curvature has less of an effect at higher subcoolings. This is most likely due to the larger contribution of single-phase heat transfer. Unlike water, and to a lesser extent R-12, FC-72 has a low latent to sensible heat ratio, 3.8 and 2.2 for $\Delta T_{sub} = 20$ and 35°C, respectively. Thus, any enhancement in boiling heat transfer will have less of an effect as subcooling is increased. For $\Delta T_{sub} = 35$°C, Fig. 9 shows that the relative degree of enhancement attributed to the various geometries is different from that for $\Delta T_{sub} = 20$°C. For this subcooling, the large radius channel shows the largest degree of enhancement. The two geometries with larger channel heights, (i.e., larger secondary flows), show the greatest degree of enhancement. At a subcooling of 35°C, the bubble departure size is the smallest and buoyancy forces will consequently have the least effect. Therefore, the positive effects of secondary flow on the significant single-phase heat transfer may outweigh the negative effects of secondary flow on nucleate boiling heat transfer. There is no explanation for the seemingly anomalous behavior at $U = 1$ m/s and $\Delta T_{sub} = 35$°C for the channel with $R = 28.6$ mm and $h = 6.35$ mm.

In summary, the positive effects of channel curvature are most pronounced at lower subcoolings where buoyant forces are the greatest. The two channels with smaller radii of curvature show the greatest enhancement at lower subcoolings, even though secondary flows and wall shear stresses would indicate otherwise. This further implies the importance of buoyant forces at lower subcoolings. At high subcooling, the positive effects of channel curvature on CHF diminish and channel curvature may even be detrimental. The positive effects of secondary flow on an increased single-phase heat transfer component appear to outweigh the negative effects of secondary flow on two-phase heat transfer at high subcooling. This implies that an optimal combination of radius of curvature and channel height exists at high subcooling.

Improved Correlation

As well-developed as Eqs. (1), (2), and (11) are, they unfortunately do not fit the data as well as desired. The fit may be improved for $We^{-1} > 10^{-4}$ and the present data by determining new constants, ψ and C_{sub}, however, for $We^{-1} < 10^{-4}$ (high velocities), the fit is still poor. Part of the problem lies with the transition from a CHF mechanism described by the physical model to one that is not. As Fig. 3 shows, CHF correlates strongly with the flow velocity. Because the fit degenerates with increasing velocity and the assumed velocity profile gives rise to the exponents of the nondimensional quantities in Eqs. (1), (2), and (11), shortcomings in the assumed form of the velocity profile were sought. A key assumption in the derivation of the correlations is that the bubble layer thickness is much greater than the thickness of the laminar sublayer, and thus, the laminar sublayer is a negligible portion of the flow feeding the liquid sublayer. Therefore, the velocity profile of the turbulent core is assumed over the thickness of the liquid sublayer δ_M. Specifically, the power-law form is assumed for the sake of simplicity. However, it is the thickness of the liquid sublayer that should perhaps be used to judge the appropriate velocity profile form. In this case the above assumption does not hold. To use a composite of the appropriate velocity profiles; laminar sublayer, buffer layer (Van Driest), and turbulent core (law of the wall), would yield a correlation so complex that it would be useless. Therefore, if Eqs. (1) and (2) are rederived using the laminar sublayer velocity profile

$$u^+ = y^+ \tag{12}$$

an extra term, $Re^{1/4}$, appears in the denominator of Eq. (2) and the exponents of the other nondimensional quantities are changed. Although this correlation alone is not applicable, the factor of $Re^{1/4}$ further implies that the velocity dependence of CHF is not well described by Eqs. (1), (2), and (11), and that their shortcomings are related to the assumed velocity profile.

Consequently, two modifications of the existing correlation with respect to velocity were explored: 1) adding the Reynolds number to the denominator of Eq. (2) and fitting an exponent to it, and 2) simply fitting a new exponent to the Weber number of Eq. (1). A weighted least-squares scheme was used to fit the new constants along with new values for ψ and C_{sub}. To determine a baseline correlation for the curved channel, only the straight channel data of $h \geq 3.18$ mm were fit. The index of correlation i_{xy} and the mean absolute percentage error were used to judge the efficacy of these modifications. The index of correlation, (a perfect fit is obtained as $i_{xy} \rightarrow 1$), was calculated only for q_M^{**} against We^{-1}. Table 3 shows that adding $Re^{0.146}$ to the denominator of Eq. (2) and finding new values for ψ and C_{sub} reduces the mean error by about 40%, whereas simply determining new values for ψ and C_{sub} reduces the mean error by only 20%. Note that the exponent of Re is of the same order as the exponent provided by the derivation of Eq. (2) using the laminar sublayer velocity profile. The bottom of Fig. 7 also shows that this modification models the data well, although the same We^{-1} independence seems to hold at higher velocities.

Unfortunately, Table 3 and the bottom of Fig. 8 show that the same modification to the curved channel correlation, Eq. (11), yields less impressive results, particularly with the correlation of q_M^{**} to We^{-1}. The plot of the data in the bottom of Fig. 8 shows that almost all the data falls above the cor-

Table 3 Correlation constants and accuracy parameters

Correlation	$1.052\psi^{8/23}$	C_{sub}	i_{xy}	$\overline{\text{Error}}$, %
Eqs. (1) and (2)	0.161	0.021	0.85	13.1
Eqs. (1) and (2)	0.120	0.049	0.88	10.7
Eq. (1) and Eq. (2)/$Re^{0.146}$	0.021	0.069	0.93	7.7
Eqs. (13) and (14)	N/A	N/A	0.96	5.7
Eqs. (1) and (11)	0.161	0.021	0.87	13.3
Eq. (1) and Eq. (11)/$Re^{0.146}$	0.021	0.069	0.75	11.4
Eqs. (13), (20), and (21)	N/A	N/A	0.99	4.5

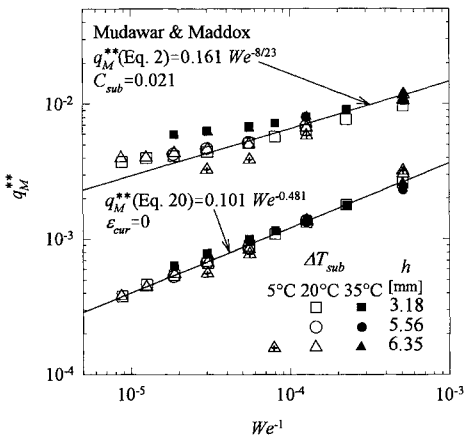

Fig. 10 Comparison of empirical straight channel correlation, Eqs. (13) and (14), with Eqs. (1–4).

relation line. Because the data fall predominantly above the prediction, but only slightly for larger subcoolings, a low i_{xy} and a low mean error are both achieved. Note that while the high subcooling data fit well, there is a glaring deficiency of the modified Eq. (11) to correlate the low subcooling data. This confirms that the effects of secondary flow are dominant at high subcooling while buoyancy is dominant at lower subcoolings. One cannot truly expect Eq. (11) to fully account for the effects of curvature since there is no buoyancy term or secondary flow term. Thus, an empirical correlation is sought.

Monde and Katto[20] considered all the independent variables that play a role in boiling and by using the Buckingham Pi theorem. The nondimensional terms of their correlation were identical to those of Eq. (2). The absence of any terms containing D_h in their correlation must be noted. The same strategy was followed to develop a correlation for the present straight channel data with a correction for channel curvature. By including D_h in the group of independent variables and neglecting the buoyancy term $g(\rho_f - \rho_g)$ and only the vapor viscosity (because Re was found to be an important factor), the following correlation was generated:

$$q_M^{**} = 0.101We^{-0.481} \tag{13}$$

where

$$q_M^{**} = \frac{q_M/U\rho_g h_{fg}}{(\rho_f/\rho_g)^{0.167}(L/D_h)^{0.310}Re^{0.336}[1 + 4.561Ja^{1.392}]} \tag{14}$$

The absence of the density ratio in the correction for subcooling is a consequence of having to fit all of the exponents at once rather than taking the approach of Monde and Katto[20] where the nonsubcooling exponents were first found for the zero subcooling data. The correlation coefficient for this equation was 0.96 and the mean absolute error was only 5.7%. Figure 10 illustrates how much better Eqs. (13) and (14) fit the data as compared to Eqs. (1) and (2). Note that Eqs. (13) and (14) provide an excellent fit throughout the range of We.

By examining an alternate form of Eq. (14), Re was found to indeed be important for correlating the high velocity data. Through examination of Eq. (14), it is apparent that D_h and, consequently, one nondimensional term, may be eliminated with little or no loss of accuracy. It is retained to maintain consistency with the following correction for channel curvature.

Channel curvature introduces one new independent variable, R. Consequently, a correction to the straight channel correlation for channel curvature is sought in a form similar to that for subcooling in the denominator of Eq. (14) since the straight channel correlation must be obtained as $R \to \infty$. Once again employing the Pi theorem with the inclusion of R and $a(\rho_f - \rho_g)$ to account for buoyancy, and neglecting the independent variables not necessary for correcting for curvature yields:

$$\text{curvature correction} = \{1 + C_{cur}Re^{\alpha_1}(D_h/2)^{\alpha_2}Ri^{\alpha_3}(\rho_f/\rho_g)^{\alpha_4}[1 + C_{buoy}Ja^{\alpha_5}]\} \tag{15}$$

Note that with the substitution of a for g in the third term on the right side, the Richardson number, that this term becomes independent of velocity. A further modification of Eq. (15) must be made because the data of Fig. 9 show that curvature is inversely proportional to the subcooling, which is represented by the last term on the right side, the Jakob number. Therefore, the exponent of the Jakob number, α_5, will be negative and the equation will not make physical sense for zero subcooling. As mentioned earlier, the effect of increasing subcooling is to reduce the bubble departure diameter, which results in reduced buoyancy forces. Furthermore, the bubble departure diameter would be more suitable than the heated length in the third term on the right side of Eq. (15). This is not correct though, because the bubble departure diameter is not an independent variable. However, the bubble departure diameter is often given by correlations of the form[21]

$$d_d \propto C[c_p(T_w - T_{sat})/h_{fg}]^{\alpha} \times \text{other terms} \tag{16}$$

As subcooling decreases, $T_w - T_{sat}$, the wall superheat, increases while the other terms in Eq. (16) change relatively little. Equation (16) thus indicates that d_d and ΔT_{sub} are inversely proportional as noted above. Because the wall superheat changes little with velocity, the following approximation may be made:

$$(T_w - T_{sat}) = -m\Delta T_{sub} + n \tag{17}$$

where m and n are positive constants. Substituting Eq. (17) into the wall superheat term of Eq. (16) gives

$$c_p(T_w - T_{sat})/h_{fg} = -mJa + nc_p/h_{fg} \tag{18}$$

where the last term on the right side may be assumed constant, for the present experiments. Equation (18) indicates the proper form for the subcooling term of Eq. (15). To simplify Eq. (15), Re and the hydraulic diameter to radius ratio were grouped

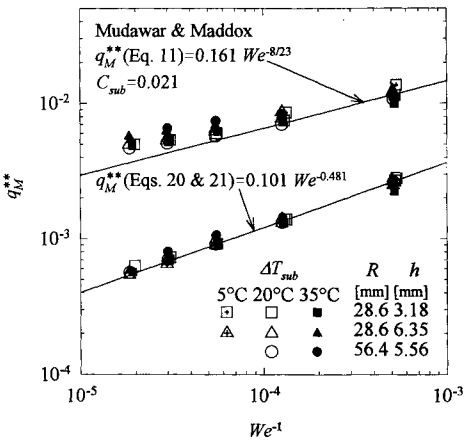

Fig. 11 Comparison of empirical curved channel correlation, Eqs. (13), (20), and (21), with Eqs. (1–4).

to give the It group found in Ito's equation, Eq. (8). Incorporating the above changes, Eq. (15) becomes

$$\text{curvature correction} = \{1 + C_{cur} It^{\alpha_1} Ri^{\alpha_2} (\rho_f/\rho_g)^{\alpha_3} [n^* - Ja]^{\alpha_4}\} \quad (19)$$

Adding this correction to the denominator of Eq. (14) and fitting the constants to the curved channel yields a correlation coefficient of 0.99 and a mean absolute error of only 4.5%. Thus, Eq. (13) is recommended for correlating all of the data of the present study where

$$q_M^{**} = \frac{q_M/U\rho_g h_{fg}}{(\rho_f/\rho_g)^{0.167}(L/D_h)^{0.310} Re^{0.336}[1 + 4.561 Ja^{1.392}](1 + \varepsilon_{cur})} \quad (20)$$

and the correction for curvature is

$$\varepsilon_{cur} = 0.086 It^{0.027} Ri^{1.013} (\rho_f/\rho_g)^{1.2062} [0.746 - Ja]^{2.251} \quad (21)$$

These correlations fit the data with an overall mean absolute error of about 5%. Figure 11 illustrates how much better this approach correlates the data than the theoretical approach taken to derive Eqs. (1) and (11).

The first two terms on the right side of Eq. (21) account for the combined effects of a changing velocity profile and the effects of secondary flow. The exponent of the It factor is about three times that of the same factor in Eq. (11). This is to be expected, Ito's[18] correlation, Eq. (8), for the friction factor was found through application of the Darcy-Weisbach equation to a circular pipe over the length of a nearly 360-deg bend. Hence, his correlation averages the entrance effects with the fully developed flow, and more importantly, also yields the average skin friction coefficient over the pipe circumference. Thus, the skin friction coefficient of the outer wall will be underpredicted and the larger exponent found for the channel curvature term is warranted. Furthermore, the effects of secondary flow were not represented by the It factor of Eq. (11). It is also interesting to note that the constant, 0.746, of Eq. (21) is nearly equal to that estimated by the use of Eq. (18) for one randomly chosen data set. Finally, Eq. (21) predicts that channel curvature will have a negative impact on CHF for sufficiently high subcooling (approximately 55°C for near atmospheric conditions).

Conclusions

1) Channel height has little effect on CHF until it reaches the same order as the bubble layer thickness. For small h, an increase of q_M at low velocities where the bubble layer is thickest may be due to an increase of velocity. A decrease of q_M for small h, at higher velocities is due to the inhibition of a more effective liquid supply mechanism.

2) Curvature of the flow path appears to offer only a moderate advantage for the geometries studied and a subcooling of 20°C or more. Channel curvature where R = 28.6 mm yields a 50% increase of q_M for a subcooling of 5°C, however. Thus, channel curvature is advantageous only when it is desired to operate near the saturation temperature.

3) Enhanced vapor removal due to increased buoyancy is the dominant mechanism responsible for increased CHF of the curved channels. The effect of buoyancy decreases with increased subcooling because of smaller bubble departure sizes at high subcoolings. A reduction in CHF may even occur for large subcooling. CHF enhancement caused by channel curvature also diminishes as subcooling increases because of the greater contribution of single-phase heat transfer for FC-72.

4) Secondary effects of an increased wall velocity gradient and secondary flows also aid in enhancing CHF. These effects begin to dominate only at very large subcoolings. An enhanced velocity profile provides higher velocity fluid near the wall for the curved channel as opposed to the straight channel. Thus, a better nucleation site liquid supply mechanism exists for the curved channel. This enhancement is nearly constant over the range of geometries and velocities investigated.

5) The lesser fit of Eqs. (1) and (2) at high velocities is probably due to neglecting the contribution of the laminar sublayer and buffer layer to the shape of the velocity profile. The We^{-1} range of validity for Eqs. (1) and (2) may be improved by inclusion of the term, $Re^{0.146}$, to the denominator of Eq. (2). The effects of channel curvature may be partially described for subcoolings greater than 20°C by the additional inclusion of the term, $It^{(1/115)}$, to the denominator of Eq. (2), [cf. Eq. (11)]. New values for the constants, ψ and C_{sub}, are provided in Table 3.

6) Equation (11) cannot account for the most dominant effect of channel curvature, enhanced vapor removal because of buoyancy. The Pi theorem was used to develop an empirical correlation for the curved channel results by first constructing a correlation for the straight channel results, Eq. (20), and then adding a correction for channel curvature, Eq. (21). The term in Eq. (21) that describes the subcooling dependence of buoyancy has rooting in the correlation of bubble departure diameter. Equations (13), (20), and (21) fit the sum total of the straight and curved channel data with a mean absolute error of about 5%.

Acknowledgments

This effort was supported by the University of Kentucky, Lexington, Kentucky, through internal funding. The authors wish to thank the 3M Industrial Products Division, St. Paul, Minnesota, for their donation of FC-72. The authors also acknowledge the efforts of Donald Brigner whose patience and diligence allowed much of the data to be obtained.

References

[1]Incropera, F. P., "Convection Heat Transfer in Electronic Equipment Cooling," *Journal of Heat Transfer*, Vol. 110, No. 4, 1988, pp. 1097–1111.

[2]Gambill, W. R., and Greene, N. D., "Boiling Burnout with Water in Vortex Flow," *Chemical Engineering Progress Symposium Series*, Vol. 54, No. 10, 1958, pp. 68–76.

[3]Leslie, B., Neukermans, A., Simon, T., and Foster, J., "Enhanced Brightness X-Ray Source," *Journal of Vacuum Science Technology B*, Vol. 1, No. 4, 1983, pp. 1251–1256.

[4]Miropol'skiy, Z. L., and Pikus, V. Yu., "Critical Boiling Heat Fluxes in Curved Channels," *Heat Transfer-Soviet Research*, Vol. 1, No. 1, 1969, pp. 74–79.

[5]Hughes, T. G., "Critical Heat Fluxes for Curved and Straight Surfaces During Subcooling Flow Boiling," M.S. Thesis, Pennsylvania State Univ., TM-74-194 (AD-A-003036), University Park, PA, Nov. 1974.

[6]Gu, C. B., Chow, L. C., and Beam, J. E., "Flow Boiling in a Curved Channel," *Heat Transfer in High Energy/High Heat Flux Applications*, American Society of Mechanical Engineers HTD-Vol. 119, 1989, pp. 25–32.

[7]Leland, J. E., and Chow, L. C., "Forced Convection Boiling from a Non-Flush Simulated Electronic Chip," *Journal of Thermophysics and Heat Transfer*, Vol. 7, No. 4, 1993, pp. 588–594.

[8]Squire, H. B., "Note on Secondary Flow in a Curved Circular Pipe," Aeronautical Research Council Rept. 16601, 1954.

[9]Rowe, M., "Measurements and Computations of Flow in Pipe Bends," *Journal of Fluid Mechanisms*, Vol. 43, No. 4, 1970, pp. 771–783.

[10]Eskinazi, S., and Yeh, H., "An Investigation on Fully Developed Turbulent Flows in a Curved Channel," *Journal of the Aeronautical Sciences*, Vol. 23, No. 1, 1956, pp. 23–34, 75.

[11]Kline, S. J., and McClintock, F. A., "Describing Uncertainties in Single-Sample Experiments," *Mechanical Engineering*, Jan. 1953, pp. 3–8.

[12]Mudawar, I., and Maddox, D. E., "Critical Heat Flux in Subcooled Flow Boiling of Fluorocarbon Liquid on a Simulated Electronic Chip in a Vertical Rectangular Channel," *International Journal of Heat and Mass Transfer*, Vol. 32, No. 2, 1989, pp. 379–394.

[13]Kenning, D. B. R., "Wall Temperature Patterns in Nucleate Boiling," *International Journal of Heat and Mass Transfer*, Vol. 35, No. 1, 1992, pp. 73–85.

[14]McGillis, W. R., Carey, V. P., and Strom, B. D., "Geometry Effects on Critical Heat Flux for Subcooled Convective Boiling from an Array of Heated Elements," *Journal of Heat Transfer*, Vol. 113, No. 2, 1991, pp. 463–471.

[15]Ulucakli, M. E., and Merte, H., Jr., "Nucleate Boiling with High Gravity and Large Subcooling," *Journal of Heat Transfer*, Vol. 112, No. 2, 1990, pp. 451–457.

[16]Marris, A. W., "Radial Distributions of Temporal-Mean Peripheral Velocity and Pressure for Fully Developed Turbulent Flow in Curved Channels," *Journal of Basic Engineering*, Vol. 82, No. 3, 1960, pp. 528–538.

[17]Ellis, L. B., and Joubert, P. N., "Turbulent Shear Flow in a Curved Duct," *Journal of Fluid Mechanics*, Vol. 62, Pt. 1, 1974, pp. 65–84.

[18]Ito, H., "Friction Factors for Turbulent Flow in Curved Pipes," *Journal of Basic Engineering*, Vol. 81, June 1959, pp. 123–134.

[19]Mudawwar, I. A., Incropera, T. A., and Incropera, F. P., "Boiling Heat Transfer and Critical Heat Flux in Liquid Films Falling on Vertically-Mounted Heat Sources," *International Journal of Heat and Mass Transfer*, Vol. 30, No. 10, 1987, pp. 2083–2095.

[20]Monde, M., and Katto, Y., "Burnout in a High Heat-Flux Boiling System with an Impinging Jet," *International Journal of Heat and Mass Transfer*, Vol. 21, No. 3, 1978, pp. 295–305.

[21]Carey, V. P., *Liquid-Vapor Phase-Change Phenomena*, Hemisphere, Washington, DC, 1992, p. 206.